All-Solution-Processed Multi-Layer White Polymer Light-Emitting Diode (WPLED) Based on the Cross-Linked [Ir(4-vb-PBI)$_2$(acac)]

Wentao Li,[†,#] Yani He,[†,#] Tiezheng Miao,[†] Xingqiang Lü,*[,†] Guorui Fu,*[,†,‡] Wai-Yeung Wong*[,‡] and Hongshan He*[,§]

[†]School of Chemical Engineering, Northwest University, Xi'an 710069, Shaanxi, China

[‡]Department of Applied Biology and Chemical Technology, The Hong Kong Polytechnic University, Hung Hom, Hong Kong, China

[§]Department of Chemistry & Biochemistry, Eastern Illinois University, Charleston, IL 61920, USA

[#]These authors contributed equally and should be considered *co*-first authors.

KEYWORDS: Divinyl-modified [Ir(C^N)$_2$(O^O)]-heteroleptic Ir(III)-complex, orthogonal materials, cross-linking Ir^{3+}-polymer, all-solution-processing, multi-layer, WPLED

ABSTRACT

All-solution-processed multi-layer white polymer light-emitting diodes (WPLEDs) are promising candidates for low-cost and large-area flexible full-color flat-panel display and solid-state lighting. However, it is still challenging to improve their performance. In this work, based on an elegant strategy of orthogonal materials, the utilization of the cross-linked Ir^{3+}-polymer film **Poly(NVK-*co*-[Ir(4-vb-PBI)$_2$(acac)]-*co*-NVK)** (**NVK** = *N*-vinyl-carbazole; **4-vb-HPBI** = 1-(4-vinylbenzyl)-2-phenyl-1*H*-benzo[*d*]imidazole and **Hacac** = acetylacetone) as the EML (emitting layer) between a hydrophilic polymer film **PEDOT:PSS** (**PEDOT:PSS** = Poly(3,4-ethylenedioxythiophene):poly(styrenesulfonate)) as the HIL (hole injection layer) and a hydrophobic polymer film **Poly(vinyl-PBD)** (**vinyl-PBD** =2-(4-(*tert*-butyl)phenyl)-5-(4'-vinyl-[1,1'-biphenyl]-4-yl)-2,5-dihydro-1,3,4-oxadiazole) as the ETL (electron transport layer), led to the successful fabrication of reliable all-solution-processed multi-layer WPLED. The device exhibits the η_{CE}^{Max} of 18.19 cd/A, the η_{PE}^{Max} of 8.16 lm/W and the η_{EQE}^{Max} of 9.32% with the stable white-lights (CIE (Commission International De L'Eclairage) coordinates *x* = 0.269-0.283, *y* = 0.317-0.330; CCTs (corrected color temperatures) of 7237-8199 K and CRIs (color rendering indices) of 63-72) under a wide applied-voltage range. Its high-performance especially with record efficiencies among those of reported all-solution-processed WPLEDs, renders cross-linking Ir^{3+}-polymers a new platform to all-solution-processed multi-layer WPLEDs.

1. INTRODUCTION

Cyclometalated Ir(III)-complexes have attracted much attention to optoelectronic (LECs (light-emitting electrochemical cells)[1] or monochromatic electro-phosphorescent device,[2-6] etc.) applications, due to their high phosphorescent efficiency and wavelength-emissive tunability associated with the ^{3}MLCT (MLCT = metal-to-ligand charge transfer) transition. Aggressively toward the practical utilizations for full-color flat-panel display and solid-state lighting,[7-10] Ir(III)-complexes-based white organic/polymer light-emitting diodes (WOLEDs/WPLEDs; vacuum-deposited WOLEDs,[11-16] solution-processed WOLEDs[17-20] and WPLEDs based on the doping[21-27] or grafting[28-33] into a polymer host) are highly concerned. The solution-processing WPLEDs[21-33] with Ir(III)-complexes-incorporated (doping[21-27] or grafting[28-33]) polymers as the emitting layers (EMLs), are more cost-effective for large-area scalable production due to high material utilization rate. In this context, one straightforward approach focused on the doping[21-27] of Ir(III)-complex-within two or multiple emitters into a polymeric matrix, from which, electric-driven di- or trichromatic color-compensation was realized for their reliable WPLEDs. However, this simple doping method suffers from a detrimental phase-separation problem,[34] thereby leading to inferior device efficiency and poor reproducibility. To circumvent these problems, an alternative is to use the grafting-typed polymer[28-33] covalently-bonded with Ir(III)-complex and/or color-compensated segments. Due to the inherent 10^3-fold higher hole mobility (10^{-3} $cm^2/V{\cdot}s$)[35] compared with electron mobility (10^{-6} $cm^2/V{\cdot}s$), most WPLEDs[21-33] fabricated by the two approaches above, were characteristic of the intricate multi-layer structure typically featuring Anode/HIL/EML/(HBL)/ETL/Cathode (HIL = hole injection layer; HBL = hole blocking

layer; ETL = electron transport layer) towards the required carriers' balance. And to avoid interference between components from dissolution or mixing during devices' fabrication, the subsequential high-vacuum vapor-depositions of small-molecule ETL and/or HBL are adopted to achieve high-efficiency with the additional casting cost.[36]

Undoubtedly, despite the great potential in further reducing that device-fabrication cost, fabrication of all-solution-processed WPLEDs including Ir(III)-complex resources, is quite challenging. Saliently, although the ETL-deprived all-solution-processed WPLEDs[37-38] configured with Anode/HIL (alcohol-soluble)/EML (hydrophobic)/Cathode were formally attempted, their certainly inferior efficiency (η_{CE}^{Max} (maximum current efficiency) = 0.0096-9.42 cd/A) with the carriers' imbalance should give place to the all-solution-processed multi-layer layout, in which, all the active layers except the electrodes (cathode and anode), must be strictly solution-deposited. During the sequential layer-by-layer deposition, no destruction of the underlying layers must be also ensured. To this end, one successful strategy[39-40] is to use an alcohol-soluble polymeric ETL to improve the efficiency (η_{CE}^{Max} = 16.6-18.5 cd/A). Unfortunately, one drawback of this strategy is that the choice of alcohol-soluble ETL polymers available for such multi-layered orthogonal-solvents system is very limited.[41] Another attractive approach is relied on an ionic transition-metal complex (iTMC; orange phosphorescence) and a color-compensated blue fluorescence polymer as the orthogonal double-emission layers (DELs).[42] However, the device showed unsatisfactory efficiency ($\eta_{CE}^{Max} < 2.0$ cd/A). The resulting white-lights are strictly limited in a narrowly applied bias voltage range of 6.0-9.0 V.

As a matter of fact, cross-linking methodology was extremely respected to the desirable

orthogonal materials. Through the specific cross-linkage by polymerization,[43] electrochemical deposition,[44] light[45] or heat[46] treatment, an insoluble polymer film could be achieved, which could enable the facilely sequential layer-by-layer depositions without interfacial erosion. The cross-linking target does not addict to one specified layer (HIL,[47] EML[48] or ETL[49] etc) during the solution-processing. This conceptual strategy of cross-linking polymers is highly praised in all-solution-processed monochromatic PLEDs[50-52] and small-molecule ETL-vacuum-deposited WPLEDs,[53] however, it has never been extending into all-solution-processing WPLEDs. In light of the unique solvent-resistance of cross-linking polymers, herein, we reported that (i) a high-efficiency cyclometalated Ir(III)-complex (**[Ir(4-vb-PBI)$_2$(acac)]**; **Scheme 1**) phosphor with as the divinyl-terminal functionality rendered its cross-linkage within a PVK (Poly(*N*-vinyl-carbazole) matrix for the phosphorescent Ir^{3+}-polymer film **Poly(NVK-*co*-[Ir(4-vb-PBI)$_2$(acac)]-*co*-NVK)** (EML; also **Scheme 1**); (ii) The covalent-bonding of the greenish-yellow-light **[Ir(4-vb-PBI)$_2$(acac)]** into the blue-light PVK created a homogeneous phase for the realization of white-lights; (iii) The implementation of orthogonal materials with the cross-linking Ir^{3+}-polymer film as the EML between a hydrophilic PEDOT:PSS as the HIL and a hydrophobic **Poly(vinyl-PBD)** (**Scheme 2**) as the ETL, led to a typically all-solution-processed multi-layer WPLED. Compared to the routine vacuum-deposited small-molecule **TPBi** (also **Scheme 2**) as the ETL in replacement for the hydrophobic **Poly(vinyl-PBD)** by spin-coating, their comparable device performance demonstrated that this conceptual strategy of cross-linking Ir^{3+}-polymers should give a new channel to their all-solution-processed multi-layer WPLEDs with high-performance.

Scheme 1. Synthesis of Vinyl-Modified 4-vb-HPBI, Divinyl-Functionalized Ir^{3+}-Complex Monomer [Ir(4-vb-PBI)$_2$(acac)] and Its Cross-Linking Ir^{3+}-Polymer Poly(NVK-*co*-[Ir(4-vb-PBI)$_2$(acac)]-*co*-NVK)

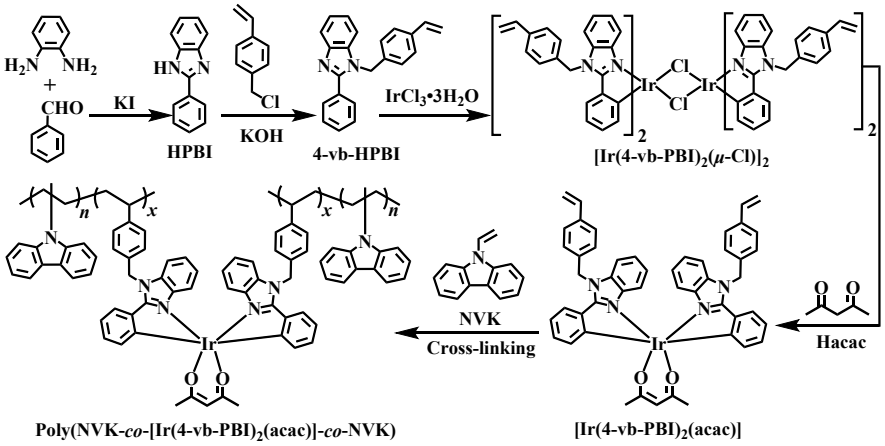

Scheme 2. Structures of Small-Molecule ETL TPBi and Polymeric ETL Poly(vinyl-PBD) through the Multi-Step Processes

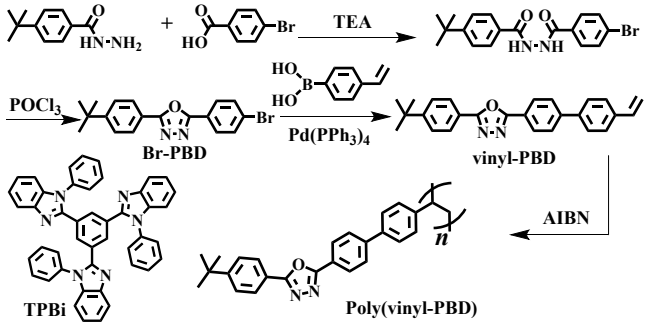

2. RESULTS AND DISCUSSION

2.1. Synthesis and Characterization of Divinyl-Functionalized Ir^{3+}-Complex Monomer [Ir(4-vb-PBI)$_2$(acac)]. The vinyl-modified ligand **4-vb-HPBI** was synthesized from the nucleophilic displacement reaction of 1-(chloromethyl)-4-vinylbenzene with the organic precursor **HPBI**[54] in the presence of KOH and Et_4NBr in 69% yield. As shown in **Scheme 1**,

treating[55] **4-vb-HPBI** with $IrCl_3.3H_2O$ in 2-ethoxyethanol and D. I. water gave rise to the μ-chloro-bridged dimer intermediate **[Ir(4-vb-PBI)$_2$Ir(μ-Cl)]$_2$**. Further reaction of this compound with **Hacac** in the presence of anhydrous Na_2CO_3, produced the divinyl-functionalized Ir^{3+}-complex monomer **[Ir(4-vb-PBI)$_2$(acac)]** in 35% yield which is soluble in common solvents except water.

The vinyl-modified ligand **4-vb-HPBI** and its divinyl-functionalized Ir^{3+}-complex monomer **[Ir(4-vb-PBI)$_2$(acac)]** were well-characterized by EA, FT-IR, ^{1}H NMR and ESI-MS. Especially in the ^{1}H NMR spectrum (**Figure S1**) of the vinyl-modified ligand **4-vb-HPBI**, the appearance of vinyl-characteristic proton resonances (δ = 6.66, 5.78 and 5.22 ppm) confirms its successful vinyl-modification. As to the its divinyl-functionalized complex monomer **[Ir(4-vb-PBI)$_2$(acac)]** (also **Figure S1**), besides the stipulated proton molar ratio of 2:1 between the deprotonated (**4-vb-PBI**)$^-$ and the (**acac**)$^-$ ligands, the almost no shifted vinyl-characteristic proton resonances (δ = 6.68, 5.79 and 5.23 ppm) compared to those of the free **4-vb-HPBI** ligand are also observed despite the coordination of Ir(III) ion. Molecular structure of **[Ir(4-vb-PBI)$_2$(acac)]**·$2CH_2Cl_2$ was determined by X-ray single-crystal diffraction analysis with the crystallographic data in **Tables S1-2**. The complex **[Ir(4-vb-PBI)$_2$(acac)]**·$2CH_2Cl_2$ crystallizes in the triclinic space group of *P-1*, where the asymmetric unit is composed of one neutral molecule **[Ir(4-vb-PBI)$_2$(acac)]** and two solvates CH_2Cl_2. As shown in **Figure 1**, two cyclometalated (**4-vb-PBI**)$^-$ ligands with the similar C^N-chelate (C51^N1 or C44^N4) mode and one (**acac**)$^-$ ligand with the O^O-chelate mode coordinate to the Ir(III)-center (Ir1) with a distorted octahedral geometry, resulting in the formation of a typical [Ir(C^N)$_2$(O^O)]-heteroleptic mononuclear framework.[56] The *trans*-N,N

and the *cis*-C,C dispositions assembled from the two cyclometalated (**4-vb-PBI**)$^-$ ligands, reveal the C_2-symmetry within the [Ir(C^N)$_2$(O^O)]-heteroleptic unit. Besides the large dihedral angle (79.2(5)° or 82.2(6)°) between the terminal vinylbenzyl ring and the benzo[*d*]imidazole plane for each (**4-vb-PBI**)$^-$ ligand, their vinyl-based modification (with the typical C=C bond lengths of 1.19(3)-1.23(3) Å) engenders the divinyl-functionalized Ir^{3+}-complex monomer **[Ir(4-vb-PBI)$_2$(acac)]** cross-linkable in the following polymerization. Thermogravimetric analysis (TGA) result (**Figure S2**) of the Ir^{3+}-complex monomer **[Ir(4-vb-PBI)$_2$(acac)]** shows its favorable thermal stability at a decomposition temperature (T_d, corresponding to 5% weight loss) up to 330 °C.

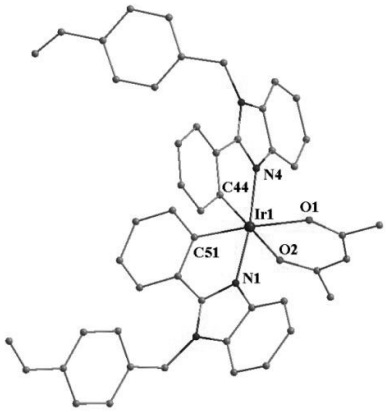

Figure 1. Perspective drawing of single-crystal structure of **[Ir(4-vb-PBI)$_2$(acac)]**·2CH_2Cl_2; H atoms and solvates CH_2Cl_2 were omitted for clarity.

2.2. Photo-Physical Property and Electronic Structure Calculation of Ir^{3+}-Complex Monomer [Ir(4-vb-PBI)$_2$(acac)]. The photo-physical property of the divinyl-functionalizedIr^{3+}-complex monomer **[Ir(4-vb-PBI)$_2$(acac)]** was examined in degassed CH_2Cl_2 solution at room temperature (RT) or 77 K and summarized in **Table S3** and **Figures**

2/**S3**. As shown in **Figure 2**, the Ir^{3+}-complex monomer **[Ir(4-vb-PBI)$_2$(acac)]** at RT shows a distinctively broadened absorption as compared to that (**Figure S3**) of the free **4-vb-HPBI** ligand: the intense absorption bands (λ_{ab} = 250 and 300 nm) within the high-energy (λ_{ab} < 350 nm) range assigned to the intraligand $^1\pi$-π^* transition, and the other relatively weak band (λ_{ab} = 386, 418 or 472 nm) extended to 500 nm probably attributed to the mixed ^{1,3}LLCT/^{1,3}MLCT (LLCT = ligand-to-ligand charge transfer) transitions. Upon excitation with λ_{ex} = 422 nm, an intense and broad emission peaking at 516 nm and a shoulder at 552 nm is observed for the Ir^{3+}-complex monomer **[Ir(4-vb-PBI)$_2$(acac)]**, giving rise to a bright yellowish-green-light with a CIE (Commission International De L'Eclairage) chromatic coordinate *x* = 0.350 and *y* = 0.592. Moreover, besides the phosphorescent nature verified by the lifetime of 2.2 μs at RT, the strong luminescence of the Ir^{3+}-complex monomer **[Ir(4-vb-PBI)$_2$(acac)]** is further confirmed from an attractive efficiency (Φ_{em}) of 43%, which is the top-level among reported yellowish-green-light Ir(III)-complexes.[57] By contrast, the almost identical emission peak positions (λ_{em} = 514 and 555 nm (sh); also **Figure S3**) with a well-resolved vibronic structure for the complex monomer **[Ir(4-vb-PBI)$_2$(acac)]** in solution at 77 K are observed. Based on the heights and energies of the 0-0 and 0-1-transitted peaks, the Huang-Rhys factor (S_M) of 0.53 relatively lower than that (0.77) at RT is estimated, indicating the complex monomer **[Ir(4-vb-PBI)$_2$(acac)]** has a weak geometric distortion[58] of the excited state relative to the ground state, which should be arisen from the intramolecular motion-suppressed relaxation.

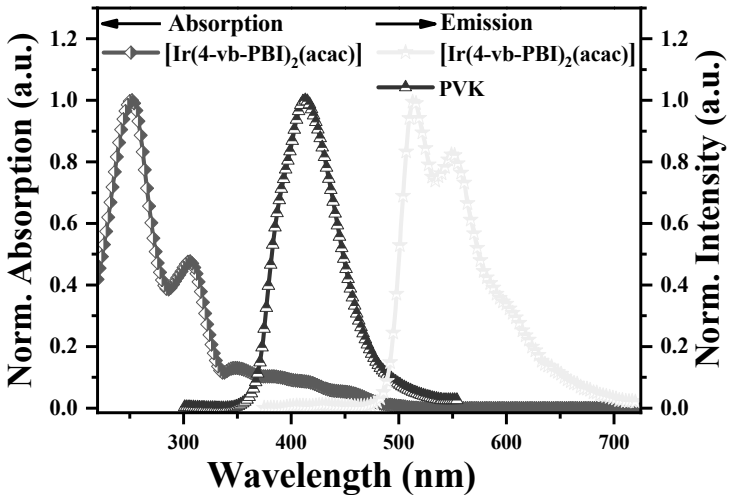

Figure 2. Normalized UV-Visible absorption and photo-luminescent spectra for the complex monomer **[Ir(4-vb-PBI)$_2$(acac)]** (λ_{ex} = 422 nm) in degassed CH_2Cl_2 solution and the PVK (λ_{ex} = 273 nm) in solid-state film at RT.

To explore the absorption nature of the Ir^{3+}-complex monomer **[Ir(4-vb-PBI)$_2$(acac)])**, time-dependent (TD) density functional theory (TD-DFT) calculations based on its optimized S_0 geometry were performed, and the results are summarized in **Table S4** and **Figure 3**. As shown in **Figure 3**, each of the LUMO, LUMO+1, LUMO+2 and LUMO+3 is almost entirely (> 96%) localized on the two (**4-vb-PBI**)$^-$ ligands with the equant contribution, while the contribution from the Ir(III)-centered d_π orbital or the π orbitals of the (**acac**)$^-$ ancillary ligand can be negligible. As to the HOMO or HOMO-2, the dominated contribution from the Ir(III)-centered d_π orbital (44.35% or 52.57%) and the two equal (**4-vb-PBI**)$^-$ ligands (25.64%×2 or 21.11%×2) endows their similar distribution pattern, and the contribution (4.37% or 5.21%) from the (**acac**)$^-$ ancillary ligand is much less. In contrast, for the HOMO-1 and HOMO-3, the contributions from the Ir(III)-centered d_π orbital (42.63%) or the π orbitals (37.31%) of the (**acac**)$^-$ ancillary ligand for the HOMO-1 while the combined (**4-vb-PBI**)$^-$

(34.33%×2) and (**acac**)$^-$ (30.39%) ligands in domination for the HOMO-3 are exhibited, despite the similar equant (10.03% or 34.33%) contribution from the two equal (**4-vb-PBI**)$^-$ ligands. Further checking from **Table S4**, the calculated $S_0 \rightarrow S_n$ (n = 1-3) transition absorptions of complex monomer **[Ir(4-vb-PBI)$_2$(acac)])** are predicted at 423, 414 and 383 nm, respectively. For the $S_0 \rightarrow S_1$ transition absorption at 423 nm, a population analysis of HOMO $\rightarrow$ LUMO+2 (77.87%) and HOMO $\rightarrow$ LUMO (19.39%) transition verifies its ^{1}MLCT-transitted nature. Two high energy-state absorptions ($S_0 \rightarrow S_n$; n = 2-3) arisen from the most HOMO or HOMO-1 $\rightarrow$ LUMO+3 transition should be characteristic of the dominated ^{1}MLCT or ^{1}MLCT/^{1}LLCT transitions, respectively. As to the $S_0 \rightarrow T_1$ absorption at 473 nm mainly reflected from the combined HOMO $\rightarrow$ LUMO+2 (59.58%), HOMO $\rightarrow$ LUMO (12.58%), HOMO-3 $\rightarrow$ LUMO+3 (9.23%), HOMO-1 $\rightarrow$ LUMO+3 (59.58%) and HOMO-2 $\rightarrow$ LUMO+2 (3.30%) transitions for complex monomer **[Ir(4-vb-PBI)$_2$(acac)])**, the triplet absorption (473 nm) can show its mixed ^{3}LLCT/^{3}MLCT-transitted (^{3}MLCT (39.94%)) character. Moreover, all the calculated absorptions featured with the mixed ^{1,3}LLCT/^{1,3}MLCT transitions are in good agreement with the experimental data (λ_{ab} = 386, 418 or 472 nm) of the complex monomer **[Ir(4-vb-PBI)$_2$(acac)])** in solution. In order to deeply elucidate its phosphorescent origin, natural transition orbitals (NTOs, **Table S4** and **Figure 4**) were further obtained for its $T_1 \rightarrow S_0$ emission with the optimized T_1 geometry, where the prevailing one (**4-vb-PBI**)$^-$-centered contribution (ca. 95%) to the NTO particle orbital while the combined (**4-vb-PBI**)$^-$-centered (71.82%) and Ir(III)-centered (23.17%) contributions to the NTO hole orbital are displayed. Hence, the almost entire percentage (98.82%) of Hole $\rightarrow$ Particle transition should suggest that the ^{3}LLCT/^{3}MLCT-admixed (^{3}MLCT (31.61%)) transitions are

responsible for its phosphorescence.

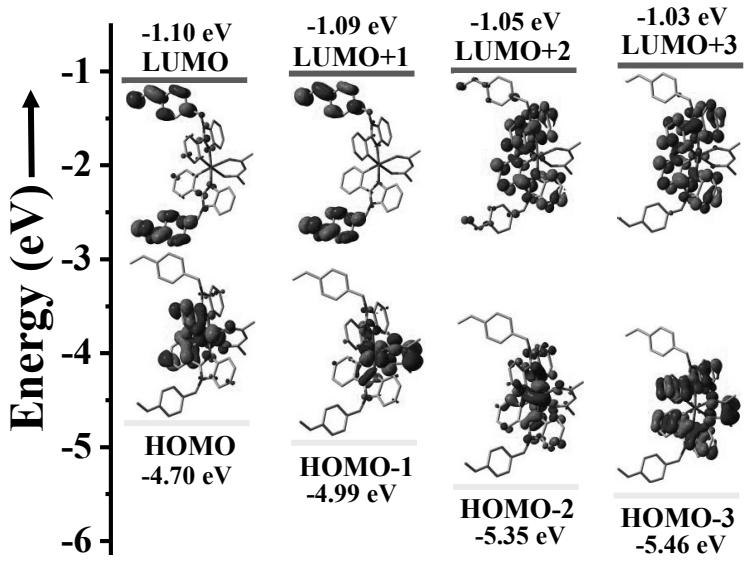

Figure 3. The HOMOs and LUMOs patterns for the Ir^{3+}-complex monomer **[Ir(4-vb-PBI)$_2$(acac)]** based on its optimized S_0 geometry.

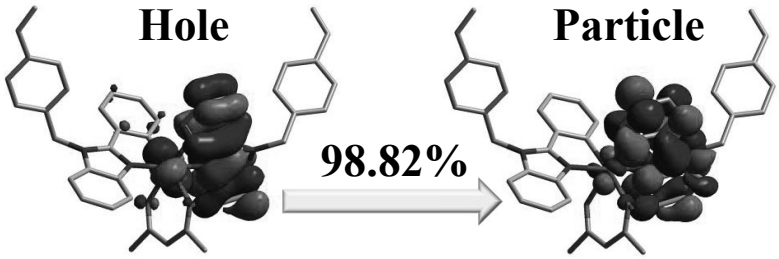

Figure 4. The NTO patterns for $T_1 \rightarrow S_0$ emission for the Ir^{3+}-complex monomer **[Ir(4-vb-PBI)$_2$(acac)]** based on its optimized T_1 geometry.

2.3. Synthesis, and Characterization of the Cross-linking Ir^{3+}-Polymer Films. To direct the cross-linking Ir^{3+}-polymeric components[59] from the Ir^{3+}-complex monomer **[Ir(4-vb-PBI)$_2$(acac)]**, cross-linking Ir^{3+}-polymer films (40 nm thickness)

Poly(NVK-*co*-[Ir(4-vb-PBI)$_2$(acac)]-*co*-NVK) (also **Scheme 1**) with the stipulated feeding (50:1, 100:1, 150:1, 200:1, 250:1 or 300:1) were synthesized by the AIBN-initiated copolymerization of NVK and the divinyl-functionalized Ir^{3+}-complex monomer **[Ir(4-vb-PBI)$_2$(acac)]**. As a matter of fact, the PVK matrix with higher energy-state blue-light can also function as both the compensation color and the energy donor to the greenish-yellow-emissive Ir^{3+}-complex monomer **[Ir(4-vb-PBI)$_2$(acac)]**, from which, effective Förster transfer energy (deduced from the significant spectral overlap between the emission of PVK and the absorption of **[Ir(4-vb-PBI)$_2$(acac)]**; also shown in **Figure 2**)[60] and desirable dichromatic white-light integration[61] should be expectable for their cross-linking Ir^{3+}-polymer films.

Due to the fully insoluble character, all the cross-linking Ir^{3+}-polymer films **Poly(NVK-*co*-[Ir(4-vb-PBI)$_2$(acac)]-*co*-NVK)** were appreciably characterized by FT-IR, XPS (X-ray photoelectron spectroscopy), PXRD (powder X-ray diffraction) and TG-DSC methods. Their XPS results show the slightly higher molar ratios of Ir(III)-complex-segments than the correspondingly initial feeding ones, probably arisen from the loss of oligomeric PVK during isolation.[62] Moreover, owing to the low-concentration grafting of the Ir^{3+}-complex monomers into the PVK matrix, each PVK-characteristic amorphous (**Figure S4**) Ir^{3+}-polymer film exhibits the high thermal stability (T_d > 400 °C and T_g about 200 °C; also **Figure S2**) as desirable. With regard to their solvent-resistance property, the DR (diffuse reflection) spectra (**Figure S5**) were investigated for the representative cross-linking Ir^{3+}-polymer film **Poly(NVK-*co*-[Ir(4-vb-PBI)$_2$(acac)]-*co*-NVK)** (250:1) by washing in 1,2-dichlorobenzene-within solvents or not at RT. Due to the covalent-grafting of the complex monomers

[Ir(4-vb-PBI)$_2$(acac)] into the PVK backbone, the cross-linking Ir^{3+}-polymer film (250:1) exhibits a slightly broader absorption band (**Figure S5**) than that of PVK. The UV-visible absorbance of the Ir^{3+}-polymer film (250:1) by washing with solvents, is almost identical to that without solvents' treatment. As a result, the no absorption reduction after washing, suggests that the required solvent-resisting property[63] is evidently realized for the cross-linking Ir^{3+}-polymer film (250:1).

The photo-luminescent properties of all the cross-linking Ir^{3+}-polymer films **Poly(NVK-*co*-[Ir(4-vb-PBI)$_2$(acac)]-*co*-NVK)** with different feedings were investigated in solid-state at RT, and the results were summarized in **Figures 5-6** and also **Table S3**. Considering the junction (also **Figure 2**) between the LLCT/MLCT absorption of **[Ir(4-vb-PBI)$_2$(acac)]** and the excitation of PVK, the λ_{ex} = 310-340 nm with every 10 nm step-size was used as the suitable excitation regime to realize their simultaneous and effective emissions. At the 50:1 feeding, photo-excitation gives rise to the dominated greenish-yellow-lights (**I-A-D**, **Figure 5(a)**; x = 0.295-0.299, y = 0.475-0.483; CCTs = 6410-6527 K and CRIs = 53-54) of **[Ir(4-vb-PBI)$_2$(acac)]**, and the PVK-based blue-light is almost quenched with the preferential energy transfer.[60] Increasing the feeding ratio to 100:1, 150:1 and to 200:1, although both the PVK-based blue-light (ca. 420 nm) and the **[Ir(4-vb-PBI)$_2$(acac)]**-centered greenish-yellow-light (516 nm) emissions are also ruled by the λ_{ex} adjustment for the three cross-linking Ir^{3+}-polymer films, the relative deficiency of the PVK-based blue-light, allows for the dichromatic-integrated colors waving from yellowish-green (**II-A-D**, **Figure 5(b)**; x = 0.306-0.311, y = 0.476-0.481; CCTs = 6095-6233 K and CRIs = 54-59) to green (**III-A-D**, **Figure 5(c)**; x = 0.277-0.282, y = 0.415-0.425; CCTs =

7188-7446 K and CRIs = 63-64; **IV-A-D**, **Figure 5(d)**; *x* = 0.274-0.281, *y* = 0.398-0.411; CCTs = 7341-7547 K and CRIs = 65-67). Convincingly, the residual while non-neglectful peak emissive at 420 nm confirms the allowance of PVK-based blue-light after the saturation of that energy transfer.[60] Interestingly, through a comparable combination for the cross-linking Ir^{3+}-polymer film **Poly(NVK-*co*-[Ir(4-vb-PBI)$_2$(acac)]-*co*-NVK)** (250:1), all the resultant dichromatic-integration color-coordinates (**V-A-D** (*x* = 0.272-0.278, *y* = 0.319-0.324); **Figure 6(a)**) locate within the desirable white-light regime, covering a broad-ranging 350-750 nm emission with 11017-12088 K of the CCTs and 76-80 of the CRIs. The obtained efficiency (Φ_{em}) up to 31.6% for the ideal white-light (*x* = 0.278, *y* = 0.324; the CCT of 11017 K and the CRI of 80) under excitation of 340 nm, is highly attractive among previously reported Ir^{3+}-doping[21-27] or Ir^{3+}-grafting[28-33] polymer systems. The 34 ns lifetime of the PVK-incorporated blue-light (λ_{em} = 420 nm) and the **[Ir(4-vb-PBI)$_2$(acac)]**-centered (λ_{em} = 516 nm) decaying lifetime of 6.8 μs, confirm that the optimal white-light for the cross-linking Ir^{3+}-polymer film (250:1) should originate from both fluorescence and phosphorescence dichromatic integration.[61] Accordingly, effective Förster transfer energy[60] (efficiency Φ_{ET} estimated from 1-(τ_{DA}/τ_D) = 12%; τ_{DA} = 38 ns; τ_D = 45 ns (λ_{em} = 440 nm) for PVK; also **Table S3**) takes place. If provided more PVK-based blue-light for the Ir^{3+}-polymer film (300:1), the excess PVK engenders the integrated white-lights (**VI-A-D** (*x* = 0.245-0.255, *y* = 0.257-0.270); **Figure 6(b)**) a significant departure, featuring the super-cool (17235-20685 K of CCTs) nature. Noticeably, except the feeding of 50:1 with a shorter phosphorescent lifetime (5.9 μs) due to aggregation-caused quenching (ACQ),[64] the **[Ir(4-vb-PBI)$_2$(acac)]**-centered greenish-yellow-light species decay with an almost constant lifetime (*ca*. 6.8 μs), whose

independence on both the other feeding (100:1~300:1) and the excitation wavelength (310-340 nm), should be attributed to the excess amount of PVK with the saturated PVK-to-**[Ir(4-vb-PBI)$_2$(acac)]** energy transfer.[60] And thus, the facilitated molecular dispersion of the **[Ir(4-vb-PBI)$_2$(acac)]**-chromophores within the PVK backbone in avoidance of unexpected self-quenching,[64] is realized especially for the cross-linking Ir^{3+}-polymer film (250:1).

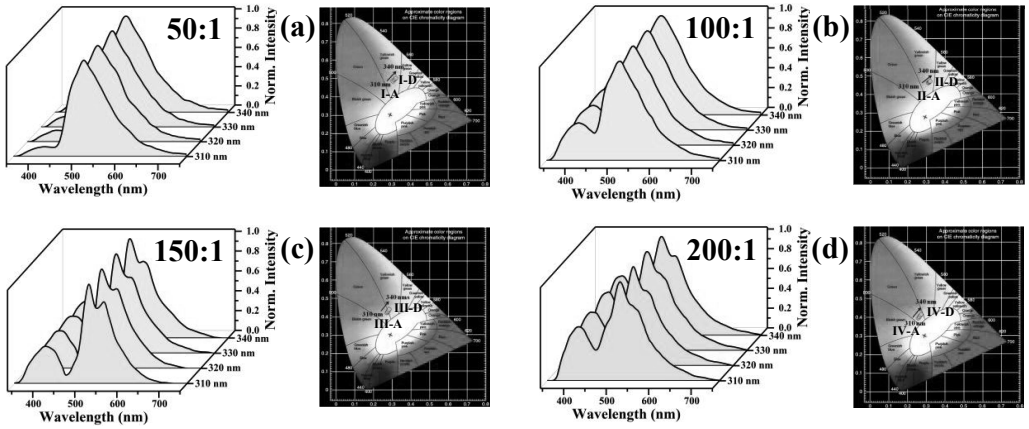

Figure 5. Normalized emission spectra (left) and corresponding CIE chromatic coordinates (right) of the cross-linking Ir^{3+}-polymeric films **Poly(NVK-*co*-[Ir(4-vb-PBI)$_2$(acac)]-*co*-NVK)** with different feedings (50:1 (a); 100:1 (b); 150:1 (c) or 200:1 (d)) upon excitation (λ_{ex} = 310-340 nm) at RT.

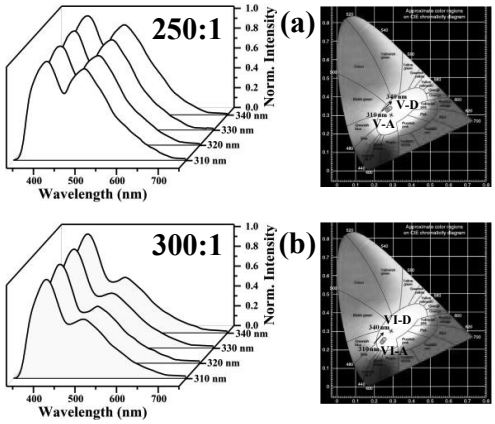

Figure 6. Normalized emission spectra (left) and corresponding CIE chromatic coordinates (right) of the cross-linking Ir^{3+}-polymeric films **Poly(NVK-*co*-[Ir(4-vb-PBI)$_2$(acac)]-*co*-NVK)** with different feedings (250:1 (a) or 300:1 (b)) upon excitation (λ_{ex} = 310-340 nm) at RT.

2.4. Synthesis and Characterization of the Polymer-typed ETL Poly(vinyl-PBD). Owing to the excellent electron-transport capability of the small-molecule **PBD** (2-(phenyl)-5-(4-*tert*-butyphenyl)-1,3,4-oxadiazole),[65] it is of special interest to obtain its derived polymer-typed ETL **Poly(vinyl-PBD)** for the following all-solution-processing. As also shown in **Scheme 2**, the vinyl-modified monomer **vinyl-PBD** was easily synthesized through the dehydration cyclization[66] and the subsequent Suzuki coupling reaction.[67] Further basing on the AIBN-initiated homogeneous polymerization of the vinyl-modified monomer **vinyl-PBD**, the polymer **Poly(vinyl-PBD)** was obtained in an acceptable yield of 90%, and whose identity was well-characterized by FT-IR, ^{1}H NMR and GPC (Gel permeation chromatography) methods. In the ^{1}H NMR spectrum (also **Figure S1**), besides the absence of the vinyl-characteristic proton resonances, the new up-shifted signals (δ = 1.57 and 1.36 ppm) of the -CH and -CH_2 groups were observed, indicating the polymer-formed effectiveness. Meanwhile, its GPC analysis of M_n = 2136 g/mol and PDI = 1.29 also verifies

the AIBN-initiated free radical polymerization. The TGA result (also **Figure S2**) shows that the polymer **Poly(vinyl-PBD)** has a high enough (T_d > 400 °C) decomposition temperature. As to its electrochemical property, the cyclic voltammetry (CV) result (**Figure S6**) of the polymer **Poly(vinyl-PBD)** shows its experimental HOMO and LUMO levels of -2.67 and -5.56 eV, respectively.

2.5. Device Fabrication and Performance of the WPLEDs-I-II with the *In Situ* Formed Cross-Linking Ir^{3+}-Polymer Films. Using the *in situ* formed cross-linking Ir^{3+}-polymer film (250:1) with the optimized straightforward white-light as the EML, a rational **WPLED-I** basing on the vacuum-deposited **TPBi** layer (30 nm) as the ETL and configuring as a non-all-solution-processed multi-layer structure (**Figure 7(a)**) of ITO/PEDOT:PSS (40 nm)/ **Poly(NVK-*co*-[Ir(4-vb-PBI)$_2$(acac)]-*co*-NVK)** (250:1; 40 nm)/**TPBi** (30 nm)/LiF (1 nm)/Al (100 nm) was fabricated for comparison. Due to the low-concentration grafting (250:1) of the cross-linking agent **[Ir(4-vb-PBI)$_2$(acac)]** (-5.11/-2.54 eV of HOMO/LUMO level checked from the corresponding CV result also in **Figure S6**) into PVK for the cross-linking Ir^{3+}-polymer film, its HOMO and LUMO levels can reasonably be identified with those (-5.50 and -2.00 eV; also **Figure S6**) of the pure PVK, respectively. According to the proposed energy-level diagram for the **WPLED-I**, the LUMO level of the cross-linking Ir^{3+}-polymer (250:1) is higher than that (-2.70 eV) of **TPBi**, while its HOMO level is lower than that (-5.20 eV) of PEDOT:PSS. Therefore, the injected electrons and holes can effectively be recombined within the Ir^{3+}-polymer EML, and subsequently carrier-trapping and color-compensation should occur.[68] As expected, the **WPLED-I** also gives the simultaneous emissions (**Figure 7(b)**) of the PVK-based blue-light (λ_{em} = 420 nm) and the **[Ir(4-vb-PBI)$_2$(acac)]**-centered

greenish-yellow-light (λ_{em} = 516 nm) throughout the whole applied bias voltage range (8.0-18.0 V). Moreover, after the turn-on voltage (V_{on} at 1 cd/m^2) of 8.5 V, their comparative combination exhibits the stable white-lights (CIE coordinates *x* = 0.266-0.275, *y* = 0.316-0.333, CCTs of 7420-8037 K and CRIs of 70-73; **Figure 7(c)**) within the illuminating 9.0-18.0 V range. Undoubtedly, in contrast to the λ_{ex}-dependent (310-340 nm) photo-excited white-lights ((CIE coordinates *x* = 0.272-0.278, *y* = 0.319-0.324, CCTs of 11017-12088 K and CRIs of 76-80; also **Table S3**) of the **Poly(NVK-*co*-[Ir(4-vb-PBI)$_2$(acac)]-*co*-NVK)** (250:1), the electroluminescent warmer (significantly lower CCTs) white-lights of the **WPLED-I** should reflect Förster energy transfer[60] and carrier-trapping[68] mechanisms concurrently conducted. As shown in **Figure 7(d)**, with an increase of the applied bias voltage, both the luminance (*L*, cd/m^2) and the current density (*J*, mA/cm^2) monotonously increase, and an L^{Max} of 315 cd/m^2 and a J^{Max} of 17.9 mA/cm^2 at 18.0 V are observed, respectively. Moreover, under the stable premise (**Figures 7(e)-7(f)**) for the **WPLED-I**, with an increase of the luminance or the applied bias voltage, all the efficiencies (η_{cE}, η_{pE} and η_{EQE}) increase first and insistently decrease (> 9.5 V) with attractive η_{CE}^{Max} = 22.02 cd/A, η_{PE}^{Max} = 8.34 lm/W and η_{EQE}^{Max} = 12.67% among previously reported Ir(III)-complex-grafting WPLEDs,[28-33] respectively. At a practical *L* of 100 cd/m^2 (16.5 V), the evident efficiency-roll-offs (*ca*. 90% with the η_{CE} = 3.37 cd/A, η_{PE} = 0.81 lm/W and η_{EQE} = 1.94%) are observed for the **WPLED-I**.

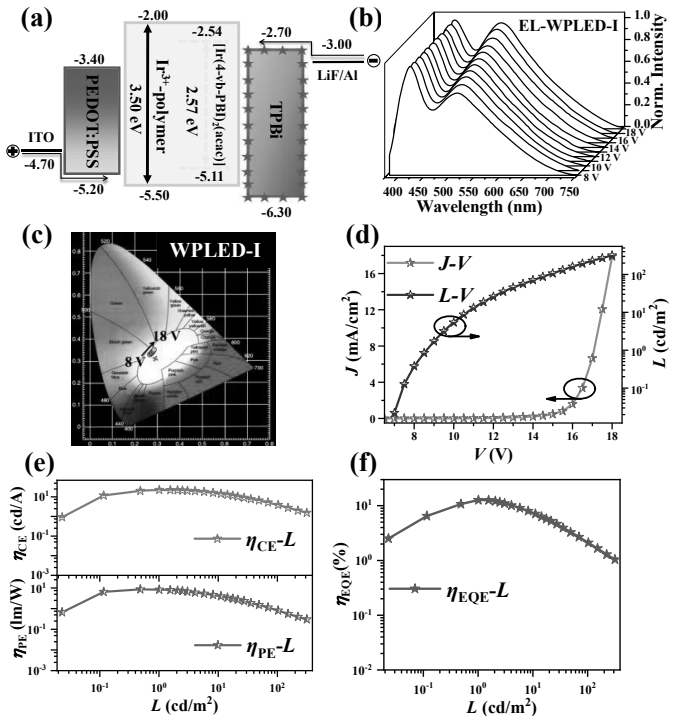

Figure 7. Device structure with energy level diagram (a); Electroluminescent spectra (b); CIE chromatic coordinates (c); *J*-*L*-*V* (d); η_{CE}-*L*, η_{PE}-*L* (e); and η_{EQE}-*L* (f) curves for the **WPLED-I** based on the vacuum-deposited **TPBi**.

Through the usage of the spin-coated **Poly(vinyl-PBD)** rather than the vacuum-deposited **TPBi** as the ETL with the same thickness (30 nm), its hydrophobic nature gives an opportunity to all-solution-processed multi-layer WPLEDs. As shown in **Figure 8(a)**, the all-solution-processed multi-layer **WPLED-II** configured with ITO/PEDOT:PSS (40 nm)/**Poly(NVK-*co*-[Ir(4-vb-PBI)$_2$(acac)]-*co*-NVK)** (250:1; 40 nm)/**Poly(vinyl-PBD)** (30 nm)/LiF (1 nm)/Al (100 nm) was successfully fabricated. Desirably, the stable dichromatic white-lights (**Figures 8(b)-8(c)**; CIE coordinates *x* = 0.269-0.283, *y* = 0.317-0.330; CCTs of 7237-8199 K and CRIs of 63-72) for the **WPLED-II** like the **WPLED-I**, are also illuminated

within that 8.0-18.0 V range, which should be arisen from the effective carrier-trapping with the HOMO/LUMO levels' stepwise alignments (**Figure 7(a)/8(a)**) of all the active layers for the **WPLEDs-I-II**. However, the intrinsic difference of the two ETLs' nature should contribute to the significantly different device performance (**Figures 8(d)-8(e)**) of the all-solution-processed multi-layer **WPLED-II**. First, the V_{on} down to 7.0 V occurs for the **WPLED-II**, which should be arisen from the lower energy barrier (0.57 eV *versus* 0.70 eV) between the LUMO levels of **Poly(NVK-*co*-[Ir(4-vb-PBI)$_2$(acac)]-*co*-NVK)** and **Poly(vinyl-PBD)** in replacement of **TPBi**. Next, the luminance (L, cd/m^2) or the current density (J, mA/cm^2) monotonously increases with an increase of the applied bias voltage for the **WPLED-II**, giving a larger L^{Max} of 494 cd/m^2 than that (L^{Max} of 315 cd/m^2) of the **WPLED-I** at the cost of a large J of 34.5 mA/cm^2 at 18.0 V. Interestingly, although the η_{CE}^{Max} of 18.19 cd/A, the η_{PE}^{Max} of 8.16 lm/W and the η_{EQE}^{Max} of 9.32% for the **WPLED-II** are slightly lower than those (η_{CE}^{Max} = 22.02 cd/A, η_{PE}^{Max} = 8.34 lm/W and η_{EQE}^{Max} = 12.67%) of the **WPLED-I**, correspondingly, the **WPLED-II** is advantageous of the significantly weaker efficiency-roll-offs (*ca*. 76% with the η_{CE} of 4.23 cd/A, the η_{PE} of 0.89 lm/W and the η_{EQE} of 2.17%) caused by the better carrier balance than that (*ca*. 90%) of the **WPLED-I** upon the J up to 100 cd/m^2. Worthy of notice, the device performance of the **WPLED-II**, together with the white-light stability, is record-renewed within reported all-solution-processed WPLEDs.[36-40, 42]

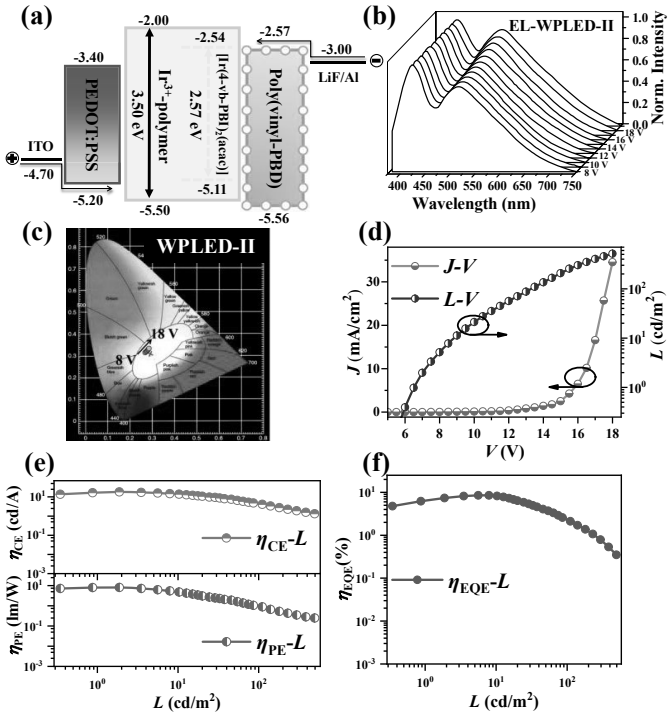

Figure 8. Device structure with energy level diagram (a); Electroluminescent spectra (b); CIE chromatic coordinates (c); *J*-*L*-*V* (d); η_{CE}-*L*, η_{PE}-*L* (e); and η_{EQE}-*L* (f) curves for the all-solution-processing multi-layer **WPLED-II** based on the spin-coated **Poly(vinyl-PBD)**.

To further explore the intrinsic carrier-trapping ability of the all-solution-processing multi-layered **WPLED-II** from the spin-coated **Poly(vinyl-PBD)** rather than the vacuum-deposited **TPBi** as the ETL, two reference devices (**Figures 9(a-b)**; **A**: ITO/LiF (1 nm)/**TPBi** (30 nm)/LiF (1 nm)/Al (100 nm); **B**: ITO/LiF (1 nm)/**Poly(vinyl-PBD)** (30 nm)/LiF (1 nm)/Al (100 nm)) were fabricated for comparison. As shown in **Figure 9(c)**, although the *J* (mA/cm^2) value for both the device **A** and the device **B** monotonously increase with the increasing of the applied bias voltage, the device **B** based on the spin-coated **Poly(vinyl-PBD)** exhibits the higher *J* sizes (2.73-80.99 mA/cm^2 for the device **B** while 2.28-68.04 mA/cm^2 for the device **A**) within the 8.0-14.0 V while distinctively lower ones after 14.0 V compared to

the device **A** with the vacuum-deposited **TPBi**. These *J-V* correlation results also reflected with those (**Figure 7-8(c)**) of the two **WPLEDs-I-II**, suggest that the facilitated electron-transport of **Poly(vinyl-PBD)** takes effect than that of **TPBi** within the 8.0-14.0 V due to the lower energy barrier (0.57 eV). Upon the further increase of the applied bias voltage from 14.0 to 18.0 V, the much stronger intermolecular interactions[69] between rigid **TPBi** dominates for the device **B** or the **WPLED-I**, from which, the higher electron mobility together with the higher electron mobility together with the additional hole-blocking ability from **TPBi** with the distinctively lower HOMO level (-6.30 eV) than that (-5.50 eV) of **Poly(vinyl-PBD)**, should contribute to the slightly higher efficiencies of the **WPLED-I** than those of the **WPLED-II** in population with more desirable carrier-traps. Meanwhile, owing to the relatively smaller energy barrier (0.30 eV) between LiF/Al and **TPBi** (-2.70 eV of the LUMO) for the **WPLED-I** than that (0.43 eV) with **Poly(vinyl-PBD)** (-2.57 eV of the LUMO) for the **WPLED-II**, the stronger electron-injecting ability across **TPBi** should be also another reason to the higher efficiencies of the **WPLED-I**. Nonetheless, the unique **WPLED-II** fabricated with the all-solution procedure, renders cross-linking Ir^{3+}-polymers a new platform to all-solution-processed multi-layered WPLEDs, and whose performance would be further improved through the following device optimization.

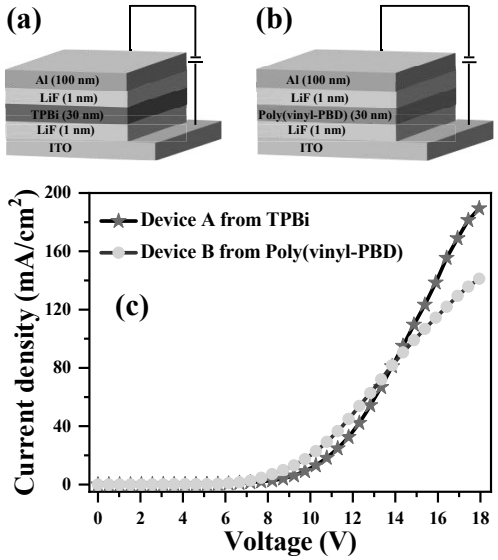

Figure 9. Device structures (a-b) and *J-V* curves (c) the reference device **A** from the vacuum-deposited **TPBi** and the reference device **B** from the spin-coated **Poly(vinyl-PBD)**.

3. CONCLUSIONS

In summary, the divinyl-modification of the Ir^{3+}-complex monomer **[Ir(4-vb-PBI)$_2$(acac)])** shows its cross-linkable nature with efficient greenish-yellow phosphorescence. Further through its *in-situ* formed cross-linking Ir^{3+}-polymer film (250:1) as the EML, the multi-layer **WPLED-I** from the vacuum-deposited **TPBi** and the all-solution-processed multi-layer **WPLED-II** from the spin-coated **Poly(vinyl-PBD)** are realized, respectively. Due to the intrinsic carrier-transport difference between **TPBi** and **Poly(vinyl-PBD)**, the device efficiencies (η_{CE}^{Max} of 18.19 cd/A, η_{PE}^{Max} of 8.16 lm/W and η_{EQE}^{Max} of 9.32%) for the **WPLED-II** are slightly lower than those (η_{CE}^{Max} = 22.02 cd/A, η_{PE}^{Max} = 8.34 lm/W and η_{EQE}^{Max} = 12.67%) of the **WPLED-I**, while the **WPLED-II** is advantageous of the significantly weaker efficiency-roll-offs. Especially, the record-renewed device performance of the **WPLED-II** among previously reported all-solution-processing WPLEDs, engenders cross-linking

Ir^{3+}-polymers a new platform to all-solution-processed multi-layer WPLEDs with high-efficiencies.

4. EXPERIMENTAL SECTION

Materials and Characterization Reagents and solvents were received from Sigma Aldrich and used without further purification. All solvents, unless otherwise stated were degassed and stored over 3 Å activated molecule sieves prior to use. All manipulations of air and water sensitive compounds were carried out under a dry N_2 atmosphere using the standard Schlenk line technique. Elemental analyses were performed on a Perkin-Elmer 240C elemental analyzer. Fourier Transform Infrared (FT-IR) spectra were recorded on a Nicolet Nagna-IR 550 spectrophotometer in the region 4000-400 cm^{-1} using KBr pellets. ^1H NMR spectra were recorded on a JEOL EX 400 spectrometer with $SiMe_4$ as internal standard in DMSO-d_6 at room temperature. ESI-MS was performed on a Finnigan LCQ^{DECA} XP HPLC-MS_n mass spectrometer with a mass to charge (*m/z*) range of 4000 using a standard electro-spray ion source and $CHCl_3$ as the solvent. Electronic absorption spectra for the solutions and diffuse reflection (DR) spectra for the solid-state polymeric films in the UV-visible region were recorded with a Cary 300 UV spectrophotometer. Visible emission and excitation spectra were collected by a combined fluorescence lifetime and steady-state spectrometer (FLS-980, Edinburgh) with a 450 W Xe lamp. Excited-state decay times were obtained by the same spectrometer but with a μF900 Xe lamp. The luminescent absolute quantum yield (Φ_{em}) in solution or solid-state was also measured by the same spectrometer using a 450 W Xe lamp and an integrating sphere. Gel permeation chromatography (GPC)

analyses of polymers were performed using a Waters 1525 binary pump coupled to a Waters 2414 refractive index detector with HPLC THF as the eluant on America Polymer Standard linear mixed bed packing columns (particle size, 10 μm). GPC was calibrated using polystyrene standards. X-ray photoelectron spectroscopy (XPS) was carried out on a PHI 5700 XPS system equipped with a dual Mg X-ray source and monochromatic Al X-ray source complete with depth profile and angle-resolved capabilities. Powder X-ray diffraction (PXRD) patterns were recorded on a D/Max-IIIA diffractometer with graphite-monochromatized Cu Kα radiation (λ = 1.5418 Å). Thermal properties were characterized using thermogravimetric (TG) and differential scanning calorimetric (DSC) analyses on a NETZSCH TG 209 instrument under flowing nitrogen at a heating rate of 10 °C/min. Synthesis of **HPBI**, **Br-PBD**, **Vinyl-PBD** and **PVK** can be found in SI.

Synthesis of the Vinyl-Modified Ligand 4-vb-HPBI. To a stirred solution of **HPBI** (194 mg; 1 mmol) in absolute DMSO (20 mL), another aqueous solution (5 mL) containing KOH (67 mg, 1.2 mmol) and Et_4NBr (210 mg, 1 mmol) was added dropwise, and the resulting mixture was continuously stirred at room temperature for 2 h. And then 1-(chloromethyl)-4-vinylbenzene (228 mg, 1.5 mmol) was added and the resultant mixture was further stirred at room temperature under a N_2 atmosphere overnight. The resulting mixture was poured into 500 mL of D. I. water for a few days to give a yellow precipitate. The crude product was filtered and further dissolved into absolute EtOH (40 mL) to give a yellow microcrystalline solid after evaporation at room temperature. Yield: 290 mg, 69%. Anal. Calcd for $C_{22}H_{18}N_2$: C, 85.13; H, 5.85; N, 9.03%. Found: C, 85.10; H, 5.93; N, 9.08%. FT-IR (KBr, cm^{-1}): 3025 (w), 2926 (w), 1597 (w), 1492 (w), 1443 (m), 1383 (w), 1328 (w), 1248 (w), 1212 (w), 1157 (m), 1128 (w),

1026 (w), 905 (m), 838 (m), 744 (vs), 691 (s), 580 (w), 563 (w), 537 (w).^{1}H NMR (400 MHz, DMSO-d_6): δ (ppm) 7.74 (m, 3H, -Ph), 7.55 (t, 3H, -Ph), 7.48 (m, 1H, -Ph), 7.39 (d, 2H, -Ph), 7.26 (m, 2H, -Ph), 6.98 (d, 2H, -Ph), 6.66 (m, 1H, =CH), 5.78 (d, 1H, =CH_2), 5.59 (s, 2H, -CH_2), 5.22 (d, 1H, =CH_2). ESI-MS (in $CHCl_3$) *m*/*z*: 311.15 (100%), $[M-H]^+$.

Synthesis of the μ-Chloro-Bridged Dimer Intermediate [Ir(4-vb-PBI)$_2$Ir(μ-Cl)]$_2$. According to the Nonoyama route,[55] to a mixed solvent of 2-ethoxyethanol and D. I. water (V/V = 3:1, 24 mL), the vinyl-modified ligand **4-vb-HPBI** (0.403 g, 1.3 mmol) and $IrCl_3 \cdot 3H_2O$ (0.208 g, 0.6 mmol) were added, and the resultant mixture was heated overnight at 110 °C under a N_2 atmosphere. After cooling to room temperature, a saturate aqueous solution (20 mL) of brine was added and the orange suspension was filtered. The orange solid was further washed with D. I. water, diethyl ether and hexane, and dried at 45 °C under vacuum to constant weight. The μ-chloro-bridged dimer intermediate **[Ir(4-vb-PBI)$_2$Ir(μ-Cl)]$_2$** was used directly for the next step without further purification. Yield: 80%.

Synthesis of the Divinyl-Functionalized Complex Monomer [Ir(4-vb-PBI)$_2$(acac)]. To a solution of the μ-chloro-bridged dimmer intermediate **[(4-vb-PBI)$_2$Ir(μ-Cl)]$_2$** (0.680 g; 0.4 mmol) in 2-ethoxyethanol (30 mL), acetylacetone (**Hacac**, 0.120 g, 1.2 mmol) and anhydrous Na_2CO_3 (0.424 g; 4.0 mmol) were added, and the reaction mixture was heated to 110 °C under a dry N_2 atmosphere for 24 h. After cooling to room temperature, saturated brine (30 mL) was added, and the resulting suspension was filtered. The crude solid was further purified by column chromatography on silica gel using *n*-Hexane/CH_2Cl_2 (V/V = 1:3) as the eluent, affording an orange microcrystalline product. Yield: 64 mg, 35%. Anal. Calcd for

$C_{49}H_{41}N_4O_2Ir$: C, 64.67; H, 4.54; N, 6.16%. Found: C, 64.55; H, 4.59; N, 6.13%. FT-IR (KBr, cm^{-1}): 3045 (w), 2961 (w), 2923 (w), 2853 (w), 1716 (w), 1629 (w), 1575 (w), 1519 (w), 1491 (w), 1445 (m), 1401 (w), 1358 (w), 1257 (m), 1198 (w), 1025 (m), 907 (m), 838 (m), 797 (vs), 723 (s), 680 (m), 580 (w), 569 (w), 536 (w). ^{1}H NMR (400 MHz, DMSO-d_6): δ (ppm): 7.84 (d, 2H, -Ph), 7.59 (d, 2H, -Ph), 7.53 (d, 2H, -Ph), 7.44 (d, 4H, -Ph), 7.38 (m, 4H, -Ph), 7.13 (d, 4H, -Ph), 6.68 (m, 4H, -Ph and =CH)), 6.50 (t, 2H, -Ph), 6.21 (m, 4H, -Ph), 6.12 (d, 2H, -Ph), 5.79 (d, 2H, $=CH_2$), 5.23 (d, 2H, $=CH_2$), 5.21 (s, 1H, =CH), 1.73 (s, 6H, $-CH_3$). ESI-MS (in $CHCl_3$) *m*/*z*: 911.29 (100%), $[M-H]^+$.

Synthesis of the AIBN-Initiated Poly(vinyl-PBD). To a solution of the organic monomer **vinyl-PBD** (3.63 g, 9.5 mmol) in dry THF (15 mL), AIBN initiator (23.4 mg, 1.5 mol% of **vinyl-PBD**) was added, and the resultant homogeneous solution was purged with N_2 for 10 min and sealed under a reduced N_2 atmosphere. The mixture was heated to 60 °C with continuous stirring for 36 h. The viscous mixture was diluted with dry THF (15 mL) and precipitated with absolute diethyl ether (50 mL) three times. The resulting solid **Poly(vinyl-PBD)** was collected by filtration and dried at 45 °C under vacuum to constant weight. For **Poly(vinyl-PBD)**: Yield: 3.30 g, 90%. FT-IR (KBr, cm^{-1}): 2962 (w), 2924 (w), 1685 (w), 1612 (m), 1583 (w), 1550 (w), 1489 (s), 1458 (w), 1404 (w), 1363 (w), 1269 (w), 1244 (m), 1182 (m), 1114 (w), 1068 (w), 1004 (m), 962 (w), 825 (vs), 752 (w), 732 (w), 711 (m), 557 (w), 476 (w).^{1}H NMR (400 MHz, DMSO-d_6): δ (ppm) 8.22-6.83 (b, 12H), 1.57 (s, 3H), 1.38 (s, 9H). GPC result: M_n = 2136 g/mol, PDI = M_w/M_n = 1.29.

Synthesis of the Cross-Linking Ir^{3+}-Polymers Poly(NVK-*co*-[Ir(4-vb-PBI)$_2$(acac)]-*co*-NVK) with Different Feedings. A mixture of NVK, the divinyl-functionalized complex monomer

[Ir(4-vb-PBI)$_2$(acac)] at a stipulated feed molar ratio (50:1, 100:1, 150:1, 200:1, 250:1 or 300:1) and the AIBN initiator (1.5 mol% of NVK) was dissolved in dry 1,2-dichlorobenzene (50 mL), and the resultant homogeneous solution was purged with N_2 for 10 min and sealed under a reduced N_2 atmosphere. The mixture was thermally treated with 180 °C for 3 h. After cooling to RT, the precipitated was filtered, washed by chlorobenzene and acetone, and then dried at 45 °C under vacuum to constant weight, affording to the cross-linked Ir^{3+}-polymers as desired, respectively. For cross-linking Ir^{3+}-polymers **Poly(NVK-*co*-[Ir(4-vb-PBI)$_2$(acac)]-*co*-NVK)**: Yield: 96-98% (50:1, 100:1, 150:1 or 200:1) and 94-96% (250:1 or 300:1). Representative (250:1) FT-IR (KBr, cm^{-1}): 3050 (w), 2926 (w), 1626 (w), 1597 (m), 1482 (m), 1448 (s), 1403 (w), 1324 (m), 1212 (w), 1156 (m), 1128 (w), 1026 (w), 907 (m), 837 (w), 743 (vs), 616 (w), 580 (w), 529 (w). The actual molar ratios' result by the XPS determination *versus* the corresponding feeding: 48:1 (50:1); 96:1 (100:1); 143:1 (150:1); 192:1 (200:1), 241:1 (250:1) or 292:1 (300:1).

Single-crystal X-Ray Diffraction Analysis. Single crystals for complex monomer **[Ir(4-vb-PBI)$_2$(acac)]**·$2CH_2Cl_2$ of suitable dimensions were mounted onto thin glass fibers. All the intensity datas were collected on a Bruker SMART CCD diffractometer (Mo-Kα radiation and λ = 0.71073 Å) in Φ and ω scan modes at 153 (2) K. Structures were solved by Direct methods followed by difference Fourier syntheses, and then refined by full-matrix least-squares techniques against F^2 using SHELXTL.[70] All other non-hydrogen atoms were refined with anisotropic thermal parameters. Absorption corrections were applied using SADABS.[71] All hydrogen atoms were placed in calculated positions and refined isotropically using a riding model. Crystallographic data, relevant atomic distances and bond angles for

the complex monomer **[Ir(4-vb-PBI)$_2$(acac)]**·2CH_2Cl_2 are presented in **Tables S1-2**, respectively. CCDC number 1945003 for the complex **[Ir(4-vb-PBI)$_2$(acac)]**·2CH_2Cl_2.

Electronic Structure Calculations. Theoretical studies on the electronic structure for the complex monomer **[Ir(4-vb-PBI)$_2$(acac)]** were carried out using density functional theory (DFT) and time-dependent DFT (TD-DFT) methods. The molecular structure was optimized at the ground state (S_0) in the gas phase. DFT calculations were conducted with the popular B3LYP functional theory. The 6-31G (d,p) basis set was applied for C, H, N, O, atoms, while effective core potentials employed for Zn atom were based on a LanL2DZ basis set.[72,73] The excited states' energies were computed by TD-DFT based on the ground-state (S_0) geometry. Additionally, the natural transition orbital (NTO) was analyzed for $S_0 \rightarrow T_1$ excitation based on the first triplet state (T_1) geometry optimized by UB3LYP. All calculations were carried out with Gaussian 09, Revision D.01 software package.[74] The electron density diagrams of molecular orbitals were obtained with the ChemOffice 2010 graphics program.

Electrochemical Determination. CV measurement was performed on a computer-controlled EG&G Potentiostat/Galvanostat model 283 at RT with a conventional three-electrode cell using a Ag/$AgNO_3$ (0.1 M) reference electrode, Pt carbon working electrode of 2 mm in diameter, and a platinum wire counter electrode. CV of the sample was performed in nitrogen-saturated dichloromethane containing 0.1 M Bu_4NPF_6 as supporting electrolyte. The CV was measured at a scan rate of 100 mV·s^{-1}. The HOMO and the LUMO energy levels of each sample are calculated according to the following equations,[75] E_{HOMO} = -(E_{OX}^{on}+ 4.8) eV, E_{LUMO} = -(E_{red}^{on}+ 4.8) eV, and where E_{OX}^{on} is the recorded onset oxidation potential of the complex, and E_{red}^{on} is the recorded onset reduction potential of the complex.

The HOMO and LUMO energy levels for the other used materials were obtained from the literatures.[76]

WPLEDs' Fabrication Based on the Cross-Linking Ir^{3+}-PolymerPoly(NVK-*co*-[Ir(4-vb-PBI)$_2$(acac)]-*co*-NVK) (250:1). A patterned ITO (indium tin oxide) coated glass substrate with a sheet resistance of 20 Ω *per* square was pre-washed with acetone, detergent, distilled (D. I.) water and isopropanol in an ultrasonic bath at 50 °C. After this cleaning cycle, the ITO glass was exposed under oxygen plasma for 20 min. PEDOT:PSS as the HIL from water solution was spin-coated (at 2000 rpm) on the ITO substrate and followed by drying in a vacuum oven at 140 °C for 20 min, giving a film of 40 nm thickness. The cross-linking Ir^{3+}-polymer **Poly(NVK-*co*-[Ir(4-vb-PBI)$_2$(acac)]-*co*-NVK)** (250:1) was *in situ* prepared as above, affording an about 40-nm-thick film with good surface smoothness as the EML on top of the PEDOT:PSS layer. For **WPLED-I** with the facilitated ETL (small-molecule **TPBi**), the **TPBi** (30 nm) was vacuum-deposited onto the EML, and then a LiF thin layer (1 nm) followed by 100 nm thickness Al capping layer was further deposited onto the **TPBi** substrate under vacuum of 5×10^{-6} Pa. For all-solution-processing multi-layered **WPLED-II** with the polymer **Poly(vinyl-PBD)** as ETL, a solution of **Poly(vinyl-PBD)** in $CHCl_3$ (at a concentration of 10 mg/mL) was spin-coated with a 30-nm-thickness onto the EML for replacement. Current density-voltage-luminance (*J*-*V*-*L*) was collected using a Keithley 2400 source meter equipped with a calibrated silicon photodiode. The electroluminescent spectra were measured by a PR655 spectrometer. The eternal quantum efficiencies (η_{EQE}) values were determined by a Si photodiode with calibration in an integration sphere (IS080, Labsphere).

ASSOCIATED CONTENT

Supporting Information

The Electronic Supporting Information (ESI) including supplemental Tables and Figures is available free of charge on the *ACS* Publications website at DOI:

AUTHOR INFORMATION

Corresponding Authors

***E-mail:** **lvxq@nwu.edu.cn** (Lü, X.)

***E-mail:** **guorui.fu@polyu.edu.hk** (Fu, G.)

***E-mail:** **wai-yeung.wong@polyu.edu.hk** (Wong, W.)

***E-mail:** **hhe@eiu.edu** (He, H.)

ORCID

Lü, X.: 0000-0001-9704-1690

Wong, W.: 0000-0002-9949-7525

He, H.: 0000-0002-7462-1366

Notes

The authors declare no conflict of interest.

ACKNOWLEDGEMENTS

Prof. Lü, X. thanks the National Natural Science Foundation (22071193, 21373160, 21173165), the Program for New Century Excellent Talents in University from the Ministry of Education of China (NCET-10-0936), the State Key Laboratory of Structure Chemistry (20190026), and the Wisteria Scientific Research Cooperation Special Project of Northwest University in P. R. of China. Prof. Wong, W. thanks the Hong Kong Polytechnic University (1-ZE1C and 847S) for the financial support.

REFERENCES

(1) Housecroft, C. E.; Constable, E. C. Over the LEC Rainbow: Color and Stability Tuning of Cyclometallated Iridium(III) Complexes in Light-Emitting Electrochemical Cells, *Coord. Chem. Rev.* **2017**, *350*, 155-177.

(2) Miao, H.; Li, G.; Shan, G.; Wang, X.; Su, Z. Recent Progress in Phosphorescent Ir(III) Complexes for Nondoped Organic Light-Emitting Diodes, *Coord. Chem. Rev.* **2020**, *413*, 213283.

(3) Li, T.; Wu, J.; Wu, Z.; Zheng, Y.; Zuo, J.; Pan, Y. Rational Design of Phosphorescent Iridium(III) Complexes for Emission Color Tunability and Their Applications in OLEDs, *Coord. Chem. Rev.* **2018**, *374*, 55-92.

(4) Henwood, A. F.; Zysman-Colman, E. Lessons Learned in Tuning the Optoelectronic Properties of Phosphorescent Iridium(III) Complexes, *Chem. Commun.* **2017**, *53*, 807-826.

(5) Tsuboi, T.; Huang, W. Recent Advances in Multicolor Emission and Color Tuning of Heteroleptic Iridium Complexes, *Israel J. Chem.* **2014**, *54*, 885-896.

(6) Ulbricht, C.; Beyer, B.; Friebe, C.; Winter, A.; Schubert, U. S. Recent Developments in the Application of Phosphorescent Iridium(III) Complex Systems, *Adv. Mater.* **2009**, *21*, 4418-4441.

(7) Ho, C.; Wong, W. Luminescent Metal-Containing Polymers for White Light Emission, *Top. Curr. Chem.* **2016**, *374*, 1-23.

(8) Ying, L.; Ho, C.; Wu, H.; Cao, Y.; Wong, W.; White Polymer Light-Emitting Devices for Solid-State Lighting: Materials, Devices, and Recent Progress, *Adv. Mater.* **2014**, *26*, 2459-2473.

(9) Yang, X.; Zhou, G.; Wong, W. Recent Design Tactics for High Performance White Polymer Light-Emitting Diodes, *J. Mater. Chem. C* **2014**, *2*, 1760-1778.

(10) Wu, H.; Ying, L.; Yang, W.; Cao, Y. Progress and Perspective of Polymer White Light-Emitting Devices and Materials, *Chem. Soc. Rev.* **2009**, *38*, 3391-3400.

(11) Miao, Y.; Tao, P.; Gao, L.; Li, X.; Wei, L.; Liu, S.; Wang, H.; Xu, B.; Zhao, Q. Highly Efficient Chlorine Functionalized Blue Iridium(III) phosphors for Blue and White Phosphorescent Organic Light-Emitting Diodes with The External Quantum Efficiency Exceeding 20%, *J. Mater. Chem. C* **2018**, *6*, 6656-6665.

(12) Tao, P.; Li, W.; Zhang, J.; Guo, S.; Zhao, Q.; Wang, H.; Wei, B.; Liu, S.; Zhou, X.; Xu, B.; Huang, W. Facile Synthesis of Highly Efficient Lepidine-Based Phosphorescent Iridium(III) Complexes for Yellow and White Organic Light-Emitting Diodes, *Adv. Funct. Mater.* **2016**, *26*, 881-894.

(13) Cao, H.; Shan, G.; Wen, X.; Sun, H.; Su, Z.; Zhong, R.; Xia, W.; Li, P.; Zhu, D. An Orange Iridium(III) Complex with Wide-Bandwidth in Electroluminescence for

Fabrication of High-Quality White Organic Light-Emitting Diodes, *J. Mater. Chem. C.* **2013**, *1*, 7371-7379.

(14) Chou, H.; Li, Y.; Chen, Y.; Chang, C.; Liao, C.; Cheng, C. New Iridium Dopants for White Phosphorescent Devices: Enhancement of Efficiency and Color Stability by an Energy-Harvesting Layer, *ACS Appl. Mater. Interfaces* **2013**, *5*, 6168-6175.

(15) Wang, R.; Liu, D.; Ren, H.; Zhang, T.; Yin, H.; Liu, G.; Li, J. Highly Efficient Orange and White Organic Light-Emitting Diodes Based on New Orange Iridium Complexes, *Adv. Mater.* **2011**, *23*, 2823-2827.

(16) Yu, X.; Kwok, H.; Wong, W. Zhou, G. Highly-Efficiency White Organic Light-Emitting Devices Based on a Highly Amorphous Iridium(III) Orange Phosphor, *Chem. Mater.* **2006**, *18*, 5097-5103.

(17) Liao, X.; Yang, X.; Zhang, R.; Cheng, J.; Li, J.; Chen, S.; Zhu, J.; Li, L. Solution-Processed Small-Molecular White Organic Light-Emitting Diodes Based on a Thermally Activated Delayed Fluorescence Dendrimer, *J. Mater. Chem. C* **2017**, *5*, 10001-10006.

(18) Deng, Y.; Cui, L.; Liu, Y.; Wang, Z.; Jiang, Z.; Liao, L. Solution-Processable Iridium Phosphor for Efficient Red and White Organic Organic Light-Emitting Diodes with Low Roll-Off, *J. Mater. Chem. C* **2016**, *4*, 1250-1256.

(19) Zhang, B.; Tan, G.; Lam, C.; Yao, B.; Ho, C.; Liu, L.; Xie, Z.; Wong, W.; Ding, J.; Wang, L. High-Efficiency Single Emissive Layer White Organic Light-Emitting Diodes Based on Solution-Processed Dendritic Host and New Orange-Emitting Iridium Complex, *Adv. Mater.* **2012**, *24*, 1873-1877.

(20) Wang, R.; Liu, D.; Zhan, R.; Deng, L.; Li, J. Solution-Processable Iridium Complexes for Efficient Orange-Red and White Organic Light-Emitting Diodes, *J. Mater. Chem.* **2012**, *22*, 1411-1417.

(21) Sarada, G.; Cho, W.; Maheshwaran, A.; Sree, V. G.; Park, H.; Gal, Y.; Song, M.; Jin, S. Deep-Blue Phosphorescent Ir(III) Complexes with Light-Harvesting Functional Moieties for Efficient Blue and White PhOLEDs in Solution-Process, *Adv. Funct. Mater.* **2017**, *27*, 1701002.

(22) Liang, A.; Huang, G.; Dong, S.; Zheng, X.; Zhu, J.; Wang, Z.; Wu, W.; Zhang, J.; Huang, F. New Iridium Complexes as Yellow Phosphorescent Emitters for Sing-Layer Yellow and White Polymer Light-Emitting Diodes, *J. Mater. Chem. C* **2016**, *4*, 6626-6633.

(23) Cho, W.; Kim, Y.; Lee, C.; Park, J.; Gal, Y.; Lee, J. W.; Jin, S. Single Emissive Layer White Phosphorescent Organic Light-Emitting Diodes Based on Solution-Processed Iridium Complexes, *Dyes Pigm.* **2014**, *108*, 115-120.

(24) Zhu, M.; Zou, J.; Hu, S.; Li, C.; Yang, C.; Wu, H.; Qin, J.; Cao, Y. Highly Efficient Single-Layer White Polymer Light-Emitting Devices Employing Triphenylamine-Based Iridium Dendritic Complexes as Orange Emissive Component, *J. Mater. Chem.* **2012**, *22*, 361-366.

(25) Zou, J.; Wu, H.; Lam, C.; Wang, C.; Zhu, J.; Zhong, C.; Hu, S.; Ho, C.; Zhou, G.; Wu, H.; Choy, W. C. H.; Peng, J.; Cao, Y.; Wang, W. Simultanous Optimization of Charge_Carrier Balance and Luminous Efficiency in Highly Efficient White Polymer Light-Emitting Devices, *Adv. Mater.* **2011**, *23*, 2976-2980.

(26) Liang, B.; Xu, Y.; Chen, Z.; Peng, J.; Cao. Y. White Polymer Phosphorescent

Light-Emitting Devices with a New Yellow-Emitting Iridium Complex Doped into Polyfluorene; *Synth. Met.* **2009**, *159*, 1876-1879.

(27) Kim, T.; Lee, H. K.; Park, O. O.; Chin, B. D.; Lee, S.; Kim, J. K. White-Light-Emitting Diodes Based on Iridium Complexes via Efficient Energy Transfer from a Conjugated Polymer, *Adv. Funct. Mater.* **2006**, *16*, 611-617.

(28) Sun, J.; Wu, D.; Gao, L.; Hou, M.; Lu, G.; Li, J.; Zhang, X.; Miao, Y.; Wang, H.; Xu. B. Polyfluorene-Based White Light Conjugated Polymers incorporating Iridium(III) Complexes: the Effect of Steric Configuration on Their Photophysical and Electroluminescent Proprties, *RSC Adv.* **2018**, *8*, 1638-1646.

(29) Guo, T.; Zhong, W.; Zou, J.; Ying, L.; Yang. W.; Peng, J. Efficient Binary White Light-Emitting Polymers Grafted with Iridium Complexes as Side Groups, *RSC Adv.* **2015**, *5*, 89888-89894.

(30) Zhu, M.; Li. Y.; Cao, X.; Jiang, B.; Wu, H.; Qin, J.; Cao, Y.; Yang, C. White Polymer Light-Emitting Light-Emitting Diodes Based on Star-Shaped Polymers with an Orange Dendritic Phosphorescent Core, *Macromol. Rapid. Commun.* **2014**, *35*, 2071-2076.

(31) Xu, F.; Kim, J.; Kim, H. U.; Jang, J.; Yook, K. S.; Lee, J. Y.; Hwang, D. Synthesis of High-Triplet-Energy Host Polymer for Blue and White Electrophosphorescent Light-Emitting Diodes, *Macromolecules* **2014**, *47*, 7397-7406.

(32) Huang, W.; Wu, Y.; Lin, H.; Lin, J. T. Electroluminescent Main-Chain Copolymers Containing Phosphorescent Benzimidazole-Based Iridium Complexes as Copolymerization Backbone Units or Dopants, *Polym. Chem.* **2010**, *1*, 494-505.

(33) Park, M.; Kwak, J.; Lee, J.; Jung, I. H.; Kong, H.; Lee, C.; Hwang, D.; Shim, H. Single Chain White Light-Emitting Polyfluorene Copolymer Containing Iridium Complex Coordination on The Main Chain, *Macromolecules* **2010**, *43*, 1379-1386.

(34) Chen, Z.; Ho, C.; Wong, W. Single-Molecular White-Light Emitters and Their Potential WOLED Applications, *Adv. Mater.* **2020**, *32*, 1903269.

(35) Gao, M.; Lee, T.; Burn, P. L.; Mark, A. E.; Pivrikas, A.; Shaw, P. E. Revealing the Interplay Between Charge Transport, Luminescent Efficiency, and Morphology in Organic Light-Emitting Diode Blends, *Adv. Funct. Mater.* **2020**, *30*, 1907942.

(36) Liu, H.; Liu, F.; Lu, P. Multiple Strategies towards High-Efficiency White Organic Light-Emitting Diodes by the Vacuum Deposition Method, *J. Mater. Chem. C* **2020**, *8*, 5636-5661.

(37) Duarte, L. G. T. A.; Germino, J. C.; Berbigier, J. F.; Barboza, C. A.; Faleiros, M. M.; Simoni, D. de A.; Galante, M. T.; Holanda, M. S. de, Rodembusch, F. S.; Atvars, T. D. Z. White-Light Generation From All-Solution-Processed OLEDs Using a Benzothiazole-Salophen Derivative Reactive to the ESIPT Process, *Phy. Chem. Chem. Phys.* **2019**, *21*, 1172-1182.

(38) Coya, C.; Alvarez, A. L.; Ramos, M.; Gomez, R.; Seoane, C.; Segura, J. L. Highly Efficient Solution-Processed White Organic Light-Emitting Diodes Based on Novel Copolymer Single Layer, *Synth. Met.* **2011**, *161*, 2580-2584.

(39) Chang, Y.-T.; Jen, T.-H.; Chen, S.-A. Voltage Independent White Emission From All Solution Processed Polymer Light-Emitting Diode with Dual Emitting Layers Spaced by an Alcohol Soluble Conjugated Polymer as Interlayer, *Org. Electron.* **2013**, *14*, 2948-2952.

(40) An, D.; Zou, J.; Wu, H.; Peng, J.; Yang, W.; Cao, Y. White Emission Polymer Light-Emitting Devices with Efficient Electron Injection from Alcohol/Water-Soluble Polymer/Al Bilayer Cathode, *Org. Electron.* **2009**, *10*, 299-304.

(41) Chen, F.; Wang, S.; Xiao, Y.; Peng, F.; Zhou, N.; Ying, L.; Li, X. Alcohol-Soluble Electron-Transport Materials for Fully Solution-Processed Green PhOLEDs, *Chem. Asian J.* **2018**, *13*, 1335-1341.

(42) Sessolo, M.; Tordera, D.; Bolink, H. J. Ionic Iridium Complex and Conjugated Polymer Used to Solution-Process a Bilayer White Light-Emitting Diode, *ACS Appl. Mater. Interfaces* **2013**, *5*, 630-634.

(43) Gao, Y.; Newland, B.; Zhou, D.; Matyjaszewski, K.; Wang, W. Controlled Polymerization of Multivinyl Monomers: Formation of Cyclizaed/Knotted Single-Chain Polymer Architectures, *Angew Chem. Int. Ed.* **2017**, *56*, 450-460.

(44) Liu, C.; Luo, H.; Shi, G.; Yang, J.; Chi, Z.; Yu, T.; Ma, Y. Luminescent Network Film Deposited Electrochemically From a Carbazole Functionalized AIE Molecule and Its Application for OLEDs, *J. Mater. Chem. C* **2015**, *3*, 3752-3759.

(45) Kaastrup, K.; Sikes, H. D. Using Photo-Initiated Polymerization Reactions to Detect Molecular Recognition, *Chem. Soc. Rev.* **2016**, *45*, 532-545.

(46) Scheutz, G. M.; Lessard, J. J.; Sims, M. B.; Sumerlin, B. S. Adaptable Crosslinks in Polymeric Materials: Resolving the Intersection of Thermoplastics and Thermosets, *J. Am. Chem. Soc.* **2019**, *141*, 16181-16196.

(47) Yoo, T. W.; Park, C.; Nguyen, T. M.; Kim, D. U.; Park, L. S. Synthesis of New Conjugated Polymer as Hole Injection Layer and Performance of OLED Devices, *Mol.*

Cryst. Liq. Cryst. **2011**, *551*, 69-77.

(48) Huang, J.; Peng, B.; Wang, W.; Ji, H.; Li, L.; Xi, K.; Lai, W,; Zhang, X.; Jia, X. Architecture of Conjugated Donor-Acceptor (D-A)-Type Polymer Films with Cross-Linked Structures, *Adv. Funct. Mater.* **2016**, *26*, 1646-1655.

(49) Gu, C.; Dong, W,; Yao, L.; Lv, Y.; Zhang, Z.; Lu, D.; Ma, Y. Cross-Linked Multifunctional Conjugated Polymers Prepared by In Situ Electrochemical Deposition for a Highly-Efficient Blue-Emitting and Electron-Transport Layer, *Adv. Mater.* **2012**, *24*, 2413-2417.

(50) Cho, W.; Reddy, S. S.; Kim, J.; Cho, Y.-R.; Jin, S.-H.; All Solution-Processed Red Organic Light-Emitting Diode Based on a New Thermal Cross-Linked Heteroleptic Ir(III) Complex, *J. Mater. Chem. C* **2018**, *6*, 11714-11721.

(51) Ma, B.; Kim, B. J.; Poulsen, D. A.; Pastine, S. J.; Fréchet, J. M. J. Multifunctional Crosslinkable Iridium Complexes as Hole Transporting/Electron Blocking and Emitting Materials for Solution-Processed Multilayer Organic Light-Emitting Diodes, *Adv. Funct. Mater.* **2009**, *19*, 1024-1031.

(52) Rehmann, N.; Ulbricht, C.; Köhnen, A.; Zacharias, P.; Gather, M. C.; Hertel, D.; Holder, E.; Meerholz, K.; Schubert, U. S. Advanced Device Architecture for Highly Efficient Organic Light-Emitting Diodes with an Orange-Emitting Crosslinkable Iridium(III) Complex, *Adv. Mater.* **2008**, *20*, 129-133.

(53) Niu, Y.-H.; Liu, M. S.; Ka, J.-W.; Bardeker, J.; Zin, M. T.; Schofield, R.; Chi, Y.; Jen, A. K.-Y. Crosslinkable Hole-Transport Layer on Conducting Polymer for High-Efficiency White Polymer Light-Emitting Diodes, *Adv. Mater.* **2007**, *19*, 300-304.

(54) Grenda, V. J.; Jones, R. E.; Gal, G.; Sletzinger, M. Novel Preparation of Benzimidazoles from N-aryamidines. New Synthesis of Thiabendazole, *J. Org. Chem.* **1965**, *30*, 2858-2859.

(55) Nonoyama, M. Synthesis of a few derivatives of cycloiridated 2-(2-thienyl)pyridine, *Bull. Chem. Soc. Jpn.* **1979**, *52*, 3749-3750.

(56) Zhao, J.; Hu, Y.; Lu, H.; Lu, Y.; Li, X. Progress on Benzimidazole-Based Iridium(III) Complexes for Applications in Phosphorescent OLEDs, *Org. Electron.* **2017**, *41*, 56-72.

(57) Fan, C.; Yang, C. Yellow/Orange Emissive Heavy-Metal Complexes as Phosphors in Monochromatic and White Organic Light-Emitting Devices, *Chem. Soc. Rev.* **2014**, 43, 6439-6469.

(58) Lai, P.; Brysacz, C. H.; Alam, M. K.; Ayoub, N. A.; Gray, T. G.; Bai, J.; Teets, T. S. Highly Efficient Red-Emitting Bis-Cyclometalated Iridium Complexes, *J. Am. Chem. Soc.* **2018**, *140*, 10198-10207.

(59) Fu, G.; Liu, L.; Li, W.; He, Y.; Miao, T.; Lü, X.; He, H. Efficient White Polymer Light-Emitting Diode (WPLED) Based on Single-Component Eu^{3+}-Tb^{3+}-Containing Metallopolymer, *Adv. Opt. Mater.* **2019**, *7*, 1900776.

(60) Fu, G.; He, Y,; Li, W.; Miao, T.; Lü, X.; He, H.; Liu, L.; Wong, W. Efficient White Polymer Light-Emitting Diodes (WPLEDs) Based on Covalent-Grafting of $[Zn_2(MP)_3(OAc)]$ into PVK, *Chem. Sci.* **2020**, *11*, 2640-2646.

(61) Pan, M.; Liao, W.; Yin, S.; Sun, S.; Su, C. Single-Phase White-Light-Emitting and Photoluminescent Color-Tuning Coordination Assemblies, *Chem. Rev.* **2018**, *118*, 8889-8935.

(62) Zhang, Z.; He, Y.; Liu, L.; Lü, X.; Zhu, X.; Wong, W.; Pan, M.; Su, C. Pure White-Light and Color-Tuning of Eu^{3+}-Gd^{3+}-Containing Metallopolymer, *Chem. Commun.* **2016**, *52*, 3713-3716.

(63) Lim, Y.; Park, Y.; Kang, Y.; Jiang, D. Y.; Kim, J. H.; Kim, J.; Sellinger, A.; Yoon, D. Y. Hole Injection/Transporting Materials Derived from Heck and Sol-Gel Chemistry for Application in Solution-Processed Organic Electronic Devices, *J. Am. Chem. Soc.* **2011**, *133*, 1375-1382.

(64) Tang, C.; Liu, X.-D.; Liu, F.; Wang, X.-L.; Xu, H.; Huang, W. Recent Progress in Polymer White Light-Emitting Materials and Devices, *Macromol. Chem. Phys.* **2013**, *241*, 314-342.

(65) Diaz-Ortiz, A.; Prieto, P.; Carrillo, J. R.; Martin, R.; Torres, I. Applications of Metal-Free 1,2,4-Trizole Derivatives in Material Science, *Curr. Org. Chem.* **2015**, *19*, 568-584.

(66) Augustine, J. K.; Vairperrumal, V.; Narasimhan, S.; Alagarsamy, P.; Radhakrishnan, A. Propylphosphonic Anhydride: an Efficient Reagent for the One-Pot Synthesis of 1,2,4-oxadiazoles, 1,3,4-oxadiazoles, and 1,3,4-thiadiazoles, *Tetrahedron* **2009**, *65*, 9989-9996.

(67) Liu, L.; Pang, M.; Chen, H.; Fu, G.; Li, B.; Lü, X.; Wang, L. Efficient and High Color-Purity Green-Light Polymer Light-Emitting Diodes (PLEDs) Based on a PVK-Supported Tb^{3+}-Containing Metallopolymer, *J. Mater. Chem. C* **2017**, *5*, 9021-9027.

(68) Xu, F.; Kim, H. U.; Kim, J.; Jung, B. J.; Grimsdale, A. C.; Hwang, D. Progress and Perspective of Iridium-Containing Phosphorescent Polymer for Light-Emitting Diodes,

Prog. Polym. Sci. **2015**, *47*, 92-121.

(69) Wu, C.; Zhong, Z.; Li, X.; Xiao, Y.; Peng, F.; Wang, Y.; Huang, Z.; Wang, S.; Ying, L. Novel Electron Transporting Materials for Highly Efficient Fully Solution-Processed Green PhOLEDs with Low Rolls-Off and Drive Voltage, *Dyes Pigm.* **2018**, *158*, 20-27.

(70) Sheldrick, G. M. *SHELXL-97*, Program for Crystal Structure Refinement, University of Göttingen, Göttingen, Germany, **1997**.

(71) Sheldrick, G. M. *SADABS*, University of Göttingen, Göttingen, Germany, **1996**

(72) Wadt, W. R.; Hay, P. J. Ab initio effective core potentials for molecular calculations, potentials for main group elements Na to Bi. *J. Chem. Phys.* **1985**, *82*, 284-298.

(73) Hay, P. J. Wadt, W. R. Ab initio effective core potentials for molecular calculations, potentials for K to Au Including the outermost core orbitals. *J. Chem. Phys.* **1985**, *82*, 299-310.

(74) Gaussian 09, Revision D.01, Frisch, M. J.; Trucks, G. W.; Schlegel, H. B.; Scuseria, G. E.; Robb, M. A.; Cheeseman, J. R.; Scalmani, G.; Barone, V.; Mennucci, B.; Petersson, G. A.; Nakatsuji, H.; Caricato, M.; Li, X.; Hratchian, H. P.; Izmaylov, A. F.; Bloino, J.; Zheng, G.; Sonnenberg, J. L.; Hada, M.; Ehara, M.; Toyota, K.; Fukuda, R.; Hasegawa, J.; Ishida, M.; Nakajima, T.; Honda, Y.; Kitao, O.; Nakai, H.; Vreven, T.; Montgomery, J. A.; Peralta, Jr., J. E.; Ogliaro, F.; Bearpark, M.; Heyd, J. J.; Brothers, E.; Kudin, K. N.; Staroverov, V. N.; Kobayashi, R.; Normand, J.; Raghavachari, K.; Rendell, A.; Burant, J. C.; Iyengar, S. S.; Tomasi, J.; Cossi, M.; Rega, N.; Millam, J. M.; Klene, M.; Knox, J. E.; Cross, J. B.; Bakken, V.; Adamo, C.; Jaramillo, J.; Gomperts, R.; Stratmann, R. E.;

Yazyev, O.; Austin, A. J.; Cammi, R.; Pomelli, C.; Ochterski, J. W.; Martin, R. L.; Morokuma, K.; Zakrzewski, V. G.; Voth, G. A.; Salvador, P.; Dannenberg, J. J.; Dapprich, S.; Daniels, A. D.; Farkas, Ö.; Foresman, J. B.; Ortiz, J. V.; Cioslowski, J.; Fox, D. J. Gaussian, Inc., Wallingford CT, **2009**.

(75) Chen, H. Y.; Chen, C. T.; Chen, C. T. Synthesis and Characterization of a New Series of Blue Fluorescent 2,6-Linked 9,10-Diphenylanthrylenephenylene Copolymers and Their Application for Polymer Light-Emitting Diodes, *Macromolecules* **2010**, *43*, 3613-3623.

(76) Zysman-Colman, E.; Ghosh, S. S.; Xie, G.; Varghese, S.; Chowdhury, M.; Sharma, N.; Cordes, D. B.; Slawin, A. M. Z.; Samuel, I. D. W. Solution-Processable Silicon Phthalocyanines in Electroluminescent and Photovoltaic Devices, *ACS Appl. Mater. Interfaces* **2016**, *8*, 9247-9253.